RESEARCH ARTICLE

A displacement-shifted vision-based hybrid particle tracking velocimetry (PTV) technique

M. Paul · W.-H. Tien · D. Dabiri

Abstract A displacement-shifted approach is introduced to the vision-based particle tracking velocimetry (VB-PTV) technique described in Lei et al. (Exp Fluids 53(5):1251–1268, 2012), using translational and angular displacements. The particle matching algorithm in VB-PTV is based on a proximity matrix, G_{ij}, which favors short distance particle matches over long distance matches. By modifying the formula used in constructing G_{ij}, particles that lie at the expected location of the match are favored. Two displacement-shifted methods are introduced: the first of which relies on particle image velocimetry estimates of particle displacements and the second of which relies on both the expected displacement and direction of the correct match to construct the proximity matrix. These displacement-shifted algorithms improve performance in high gradient (0.3 px/px and above), high displacement flows (upwards of 20 pixels), broadening the range of flows for which VB-PTV can be used. RMS errors in PTV results are reduced by 33 % or more when these displacement-shifted algorithms are made to the VB-PTV algorithm which is used to process Oseen vortex images. Experimental images of shear layer and the wake region of vortex shedding were used to verify the performances of the proposed methods, and the results are in agreement with the synthetic tests.

This article is part of the Topical Collection on Application of Laser Techniques to Fluid Mechanics 2012.

M. Paul · W.-H. Tien · D. Dabiri (✉)
Department of Aeronautics and Astronautics, University of Washington, Seattle, WA 98195, USA
e-mail: dabiri@aa.washington.edu

1 Introduction

Particle velocimetry refers to that body of techniques whose goal is the attainment of an instantaneous velocity vector field through the measurement of displacements of particles within a fluid in motion. Two important methods within the field of particle velocimetry are particle image velocimetry (PIV), in which velocities are obtained by correlation of a window containing multiple particle images, and particle tracking velocimetry (PTV), in which displacements of individual particles are measured. Descriptions of PIV techniques can be found in, for example, Raffel et al. (1998), Dabiri (2006), and Adrian and Westerweel (2011), and an overview of the development of particle tracking techniques is given in Lei et al. (2012). In that paper, a new particle tracking technique is developed which uses a feature association algorithm from computer vision theory (Scott and Longuet-Higgins 1991) which is guided by PIV results. The concept of considering the matching process as a global optimization process is similar to the cellular neural network PTV approach (Ohmi and Sapkota 2006), but differs in the choice of cost function and mathematics to minimize the cost function. Details of this method will be described shortly, but it was found that the performance of this technique suffered in high flow gradients (0.3 pixels/pixel and higher), especially when large particle displacements, up to 25 pixels, were present. This displacement in pixel corresponds to a ratio of mean interparticle spacing to the absolute displacement $d*$ of 0.23. Two displacement-shifted methods are presented here which reduce this degradation of performance in shearing flows and improve overall matching performance.

The original vision-based PTV technique is described in Sect. 2. The displacement-shifted methods are proposed in Sect. 3. Synthetic images are processed, and the

performances of the displacement-shifted matching techniques are compared with the original in Sect. 4. Conclusions and recommendations are made in Sect. 5.

2 Vision-based PTV

The particle tracking technique described in Lei et al. (2012) and here called vision-based PTV (VB-PTV) relies on three principles from the field of computer vision when matching particle images in multiple image frames: the principles of proximity, exclusion, and similarity. The principle of proximity states that a shorter distance match is preferred to a long one; the principle of exclusion requires one-to-one mapping between features in multiple frames, and the principle or constraint of similarity prefers matches which appear similar. The original technique from Scott and Longuet-Higgins (1991) applies the principles of proximity and exclusion, and Pilu (1997) recommends the constraint of similarity. These are adapted to particle tracking in the following way (Lei et al. 2012). After particles have been identified, there will be two lists of particle coordinates. For clarity, a naming convention is introduced. Typically, two successive images are processed in the matching algorithm. Particle images in frame 1 will be called target particles, and potential matches in frame 2 will be called candidate particles. The lists of coordinates of target and candidate particles are used to construct what has been dubbed the "proximity matrix", G_{ij}, found using the inverse Gaussian weighted distance between all target and candidate particles:

$$G_{ij} = e^{-r_{ij}^2/2\sigma^2} \tag{1}$$

Here, r_{ij} is the distance between particles i and j, and σ is the "characteristic distance" which was determined using twice the local displacement as determined by interpolating PIV results to a target particle's location. This results in a $m \times n$ matrix where m is the number of target particles and n the number of candidate particles. This matrix provides the principle of proximity. If particles i and j have no displacement between them, element G_{ij} will be unity, and if they are far from one another, element G_{ij} will be essentially zero. This matrix was modified using the constraint of similarity, per Pilu (1997), by including a cross-correlation term, C_{ij}. Windows, with dimensions $W \times W$, of the pixel intensities around each target and candidate particle are correlated, and the results are reflected in a "similarity matrix", C_{ij}.

$$C_{ij} = \frac{\sum_{u=1}^{W}\sum_{v=1}^{W}\left(I_A(u,v) - \overline{I}_A\right) \cdot \left(I_B(u,v) - \overline{I}_B\right)}{W^2 \cdot \Sigma(I_A) \cdot \Sigma(I_B)} \tag{2}$$

$\overline{I}_A$ and $\overline{I}_B$ are the mean pixel intensities within each correlation window, and $\Sigma(I_A)$ and $\Sigma(I_B)$ are the standard deviations (not summations; a capital sigma is used to avoid confusion with the characteristic distance) of those pixel intensities. The value of C_{ij} can range from -1 for a completely uncorrelated candidate feature to 1 for an identical feature. This can be incorporated into the proximity matrix:

$$G'_{ij} = G \cdot e^{\frac{-(C_{ij}-1)^2}{2\gamma^2}}. \tag{3}$$

In this formulation, the similarity coefficient is Gaussian weighted, where γ is a correlation parameter which controls the rate of decay of similarity weighting. This value is set to 0.4, per Pilu (1997). This modification reduces the impact of rogue features (particles moving in and out of the image plane) and produces more valid matches than the original algorithm. This method is similar to the initial probability estimation of the disparity proposed by Barnard and Thompson (1980). The difference is that in the current work, the cross-correlation has a different mathematical form.

This displacement-shifted proximity matrix is used to construct the "pairing matrix", which is used to determine matches, by performing singular value decomposition.

$$G' = TDU. \tag{4}$$

T and U are orthogonal matrices, and D is a non-negative diagonal matrix with the same dimensions as G. The matrix D is replaced with a rectangular identity matrix of the same dimensions and used to find the pairing matrix

$$P = TIU. \tag{5}$$

This technique results in the orthogonal pairing matrix P, which maximizes the inner product $P:G$. This matrix is used to find matched features. If an element P_{ij} is the maximum of the ith row and jth column, then particles i and j are considered matches. The mutually orthogonal rows of the P matrix tend to disallow a strong correspondence between one target feature with more than one candidate feature, or vice versa. In this way, the exclusion principle is satisfied without explicitly enforcing it, as has been done in other similar vision methods (Ullman 1979). This technique was implemented iteratively along with an outlier detection scheme (Duncan et al. 2010) used to validate matches. For further mathematical details, the reader is directed to Scott and Longuet-Higgins (1991) as well as Schonemann (1966). For further details on the VB-PTV technique, including the particle identification algorithm, the reader is referred to Lei et al. (2012).

When the VB-PTV technique was used to process synthetic images, it showed robust performance. The measures of performance were RMS error, given as the root-mean-square error of particle displacements when compared to the analytic solution, as well as match yield and reliability, given as percentages and defined in the following way:

$$E_Y = \frac{n}{v} \tag{6}$$

$$E_R = \frac{n}{d} \tag{7}$$

Match yield, E_Y, is the number of correct matches over the number of possible matches, and reliability, E_R, is the number of correct matches over the total number of matches made. A match is considered correct if it lies within 1 pixel of the true solution. That is, in a synthetic image with a known flow profile, the true displacement of a target particle in frame 1 can be calculated and the correct location of its corresponding candidate particle in frame 2 determined. If the matched candidate particle is within 1 pixel of the true match's location, that match is considered correct. Additionally, two basic types of tests were performed in Lei et al. (2012): those using known particle locations and those using unknown particle locations. In the former, lists of exact coordinates of particle images are fed into the matching algorithm. This is essentially a way of isolating the performance of the matching algorithm independently from a particle finding algorithm. In the unknown particle location tests, images are processed by the particle location algorithm and the resulting particle coordinates, which will contain inaccuracies, are fed into the matching algorithm.

Typically, the VB-PTV algorithm was able to achieve reliabilities of over 98 % and RMS errors below 0.3 pixels for a variety of flows. Match yields varied more, but were generally above 80 %. It was found, however, that the VB-PTV technique suffered a drop-off in yield and reliability and a rise in RMS error in highly shearing flows. It was also found that this performance was worsened by the presence of large displacements. Synthetic images were processed with regions of uniform gradient (from 0.1 to 0.5

px/px) and different maximum velocities (± 7 and ± 25 pixels, $d^* = 0.82$ and 0.23), using known particle locations. The results from Lei et al. (2012) are shown in Fig. 1. While reliability tended to remain above 98 %, the flow gradients caused RMS errors to rise to around 0.3 pixels when displacements of up to 7 pixels ($d^* = 0.82$) were present and over 0.7 pixels when larger displacements were present. The match yield also dropped significantly at high gradients in the presence of large displacements. In light of this performance, the displacement-shifted modifications to the matching algorithm used in VB-PTV are proposed.

3 Displacement-shifted matching

It was seen that the current tracking algorithm's performance suffered in high displacement, high gradient flows. Figure 1 shows that errors increased and match yield and reliability percentages dropped as flow gradients increased, and this was more pronounced when the flow contained larger displacements. To address this, the Scott and Longuet-Higgins (1991) method of constructing a proximity matrix is re-examined. The formula for the proximity matrix is repeated below,

$$G_{ij} = e^{-r_{ij}^2/2\sigma^2} \tag{1}$$

This matching method was designed for computer vision and might be used to match features in stereo images. Its strength lays in its simplicity and generality, as it required only one user defined parameter—the characteristic distance σ—which itself did not require a great deal of precision. Results were roughly the same so long as σ was representative of the mean displacement between features,
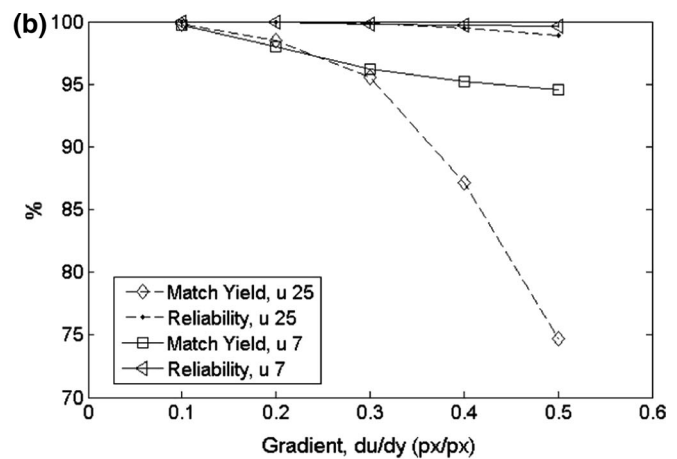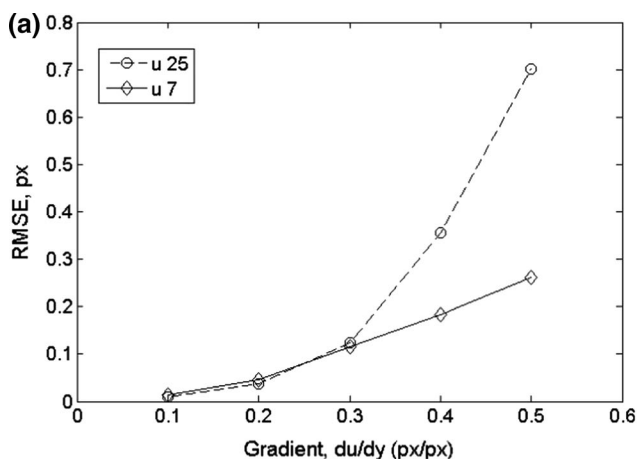

Fig. 1 a RMS error, and **b** percent yield and reliability versus flow gradient for uniform shearing flow. Flows containing maximum displacements of ± 7 ($d^* = 0.82$) and ± 25 pixels ($d^* = 0.23$) are compared. The PTV matching is guided both by PIV and exact analytic solutions (Lei et al. 2012)

and preferably an overestimate of this value. Scott and Longuet-Higgins explain that features in successive images will often be related by a transformation which is affine or nearly so. They show that when one set of points is mapped into another by a translation, expansion, or shear deformation, the 1:1 mapping minimizes the sum of squares of distances between the sets of points. And they argue that by choosing a sufficiently large σ, their matching method possesses this same property and thus is useful in discerning the many and varied transformations which exist between feature sets in image pairs. Here, a more graphical view is taken of the matching method with emphasis on the construction of the proximity matrix, G_{ij}. The process of performing singular value decomposition on this matrix to obtain a pairing matrix P_{ij} is unchanged, and so the properties that allow for robust matching remain.

We can imagine a Gaussian "proximity surface" existing around each target particle j in frame 1, described by Eq. 1, which can be thought of as a measure of a location's proximity to a target particle. This surface reaches a maximum of 1 when r_{ij} is zero and decreases monotonically as r_{ij} increases (see Fig. 2). A candidate particle i in frame two will have some value depending on where it falls on this proximity surface. This value is element G_{ij}. Since the proximity matrix is constructed using the principle of proximity, candidate particles which are closer to the target particle (that is, they experienced a smaller displacement) will have a larger element G_{ij}. If the proximity matrix were used on its own for matching by selecting elements with the largest values in given rows and columns, it would result in a nearest neighbor method. The parameter σ controls the rate of decay or the breadth of this Gaussian surface. When σ is small, the surface is small and only candidate particles near the target particle will have large values in the pairing matrix G. When σ is large, the Gaussian surface widens and more candidate particles will
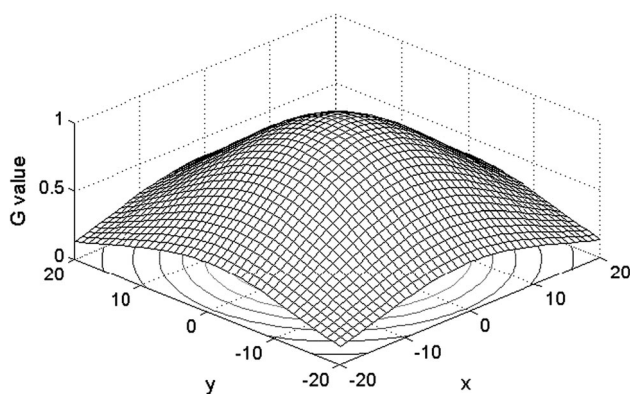

Fig. 2 Gaussian proximity surface from original Scott and Longuet-Higgins method

have large values. The process of creating a pairing matrix P permits the correct match to be found in most cases because matching is performed on all particles at once and coherent particle motion is preferred to simply matching a target particle with its nearest candidate. However, reliance on this formulation of the proximity matrix introduces unnecessary noise to the matching process, especially for large displacements. Two simple displacement-shifted modifications to G_{ij} are proposed here.

Because an estimate of local displacements can be obtained from PIV to provide guidance to the matching process, a more selective proximity matrix can be constructed. In the first modification, the proximity matrix is created using the following formula:

$$G_{ij} = e^{-(r_{ij} - r_{\text{PIV}})^2/2\varepsilon^2} \tag{8}$$

Instead of favoring candidate particles with zero displacement ($r_{ij} = 0$), the new proximity surface reaches a maximum when r_{ij} is equal to the displacement predicted by PIV, r_{PIV}, resulting in a ring-like proximity surface. This modification, which is guided by expected displacements, will be referred to as modification D1. In the second modification, the expected direction as well as displacement is taken into account.

$$G_{ij} = e^{-\left[(r_{ij} - r_{\text{PIV}})^2/2\varepsilon^2\right]} * e^{-\left\{\left[\left(\tan^{-1}\frac{dy_{ij}}{dx_{ij}}\right)^2 - \left(\tan^{-1}\frac{dy_{\text{PIV}}}{dx_{\text{PIV}}}\right)^2\right]/2\varphi^2\right\}} \tag{9}$$

The terms dy_{ij} and dx_{ij} are the pixel distances between target particle i and candidate particle j. The dy_{PIV} and dx_{PIV} terms represent the x and y displacements of target particle i predicted by PIV. The second exponential term in Eq. 9 provides a comparison between a candidate particle's angle in relation to the target particle and the PIV prediction of the angle of a target particle's displacement. The resulting proximity surface contains a peak in each quadrant, one of which will lie at the expected location of the target particle's matching candidate particle. The scaling parameters ε and φ are discussed later. This modification, based on displacement and directional guidance, will be referred to as modification D2. For comparison, proximity surfaces for a predicted displacement of 7 pixels ($d* = 0.82$) at 45° above the x-axis are shown in Figs. 2, 3, 4.

It can be seen from the above figures that the original method can result in many candidate particles with large values in the proximity matrix, while the displacement-shifted methods are far more selective and will result in a more sparse proximity matrix. This becomes more pronounced with larger predicted displacements. Like the original Gaussian proximity surface, the ring-like shape of the first displacement-shifted method and the peaks in the
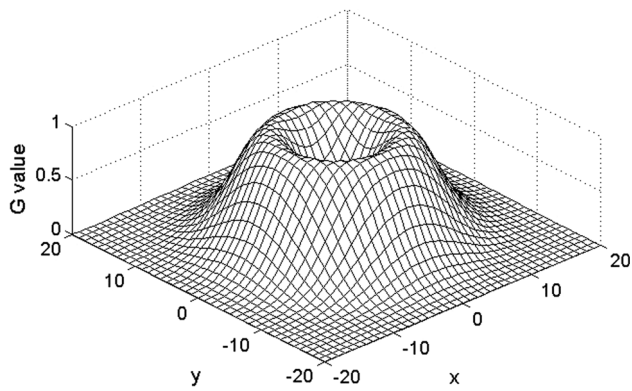
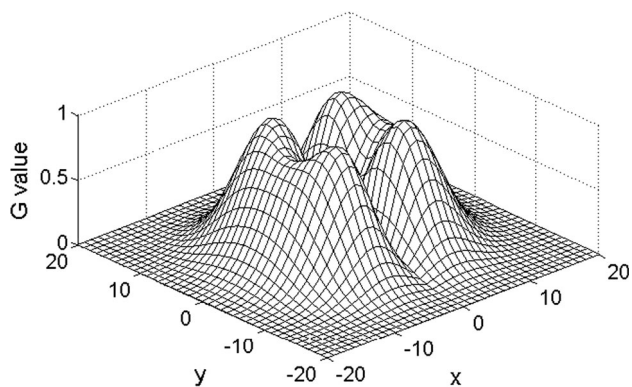**Fig. 3** Proximity surface from mod-D1, using displacement guidance

Fig. 4 Proximity surface from mod-D2 using displacement and directional guidance

second method can be widened or narrowed by controlling the parameters ε and φ. In the following results, ε was set to a value of 4. This was found to be the optimum value for high gradient flows and performed well in all other tested flows. If this parameter were made to be adaptive, it might be related to the estimated error between the predicted displacement, as found by PIV, and the true particle displacement. The parameter φ is set to unity and could similarly be related to the error between the flow direction as estimated by PIV and the actual flow direction. The proximity matrix created using Eqs. 8 or 9 is still combined with the correlation term, per Eq. 3, before it undergoes singular value decomposition.

Since both modifications are aimed at increasing the selectivity of the guidance PIV, the accuracy of the guidance PIV becomes an important factor to the tracking results. In general, the recommended interrogation window should contain 6–10 particle images for a reliable PIV cross-correlation operation. In the current study, the interrogation window size of the guidance PIV is set to 16 by 16

pixel, and the particle image density is 0.03 particles/per pixel. The resulting averaged particle number in each interrogation window is 7.67, which is in the medium range and still appropriate for the PIV algorithm to work. In practice, the values of ε and φ are used to control the sensitivity of the proximity surface to the PIV guidance, and the optimized values are related to the ability of the PIV guidance to resolve the velocity gradient. The PIV guidance that follows the local flow velocity provides better initial estimation, and therefore more chances for the correct matching pairs to have high G_{ij} values in the proximity surface to be picked up by the tracking algorithm. Since the PIV window size is usually set toward the maximum achievable resolution, the judgment of a good choice of ε and φ values would be to achieve least amount of outliers and most matches. More matched vectors indicate good matching yield, and less outliers indicate a higher reliability of the tracking results.

4 Results from synthetic images

These displacement-shifted methods were used to process many of the same synthetic flows described in Lei, et al. (2012). Since the modifications were initially produced in response to errors seen in VB-PTV performed on high gradient flow, results from uniform shearing flows are presented first.

It can be seen in Fig. 5 that the displacement-shifted methods have little effect on RMS error, match yield, and reliability when compared with the original matching algorithm's performance on shearing flow with displacements of up to ± 7 pixels ($d^* = 0.82$). The improvement can be seen by looking at Fig. 6, which shows results from shearing flows with displacements of up to ± 25 pixels ($d^* = 0.23$). Both displacement-shifted methods lower error and increase yield and reliability, and the second displacement-shifted method provides the most improvement. As much as 60 % of the RMS error is removed by the second displacement-shifted method, match yield is increased by up to 24 %. Even the already high reliability percentage is improved with the displacement-shifted approach, only dropping to 99.6, versus 98.86 % using the original method, at a shear of 0.5 px/px. The second displacement-shifted results in an error curve which resembles that for the small displacement shearing flow, with a maximum RMS error of roughly 0.3 px at high shear stress values. It would therefore seem that this improved approach reduces the error induced by large displacements in shearing flow, though not the errors induced by high gradients themselves. Given these improvements, the displacement-shifted matching methods are applied to other more complicated synthetic flows.
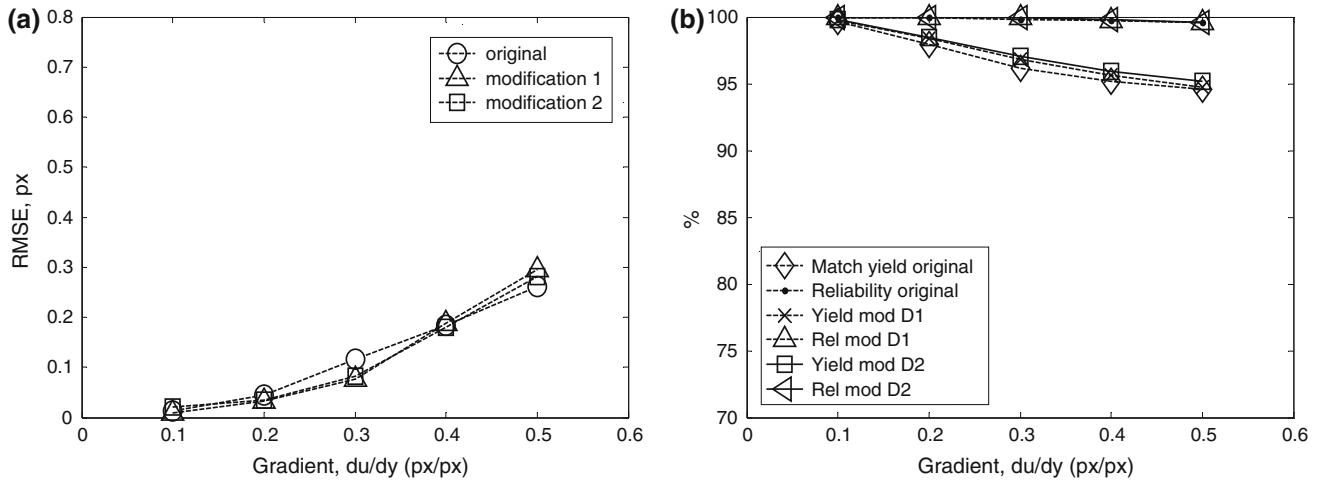
Fig. 5 a RMS error versus flow gradient with a maximum velocity of 7 pixels ($d^* = 0.82$), and **b** match yield and reliability percentages versus gradient using the original and displacement-shifted matching methods
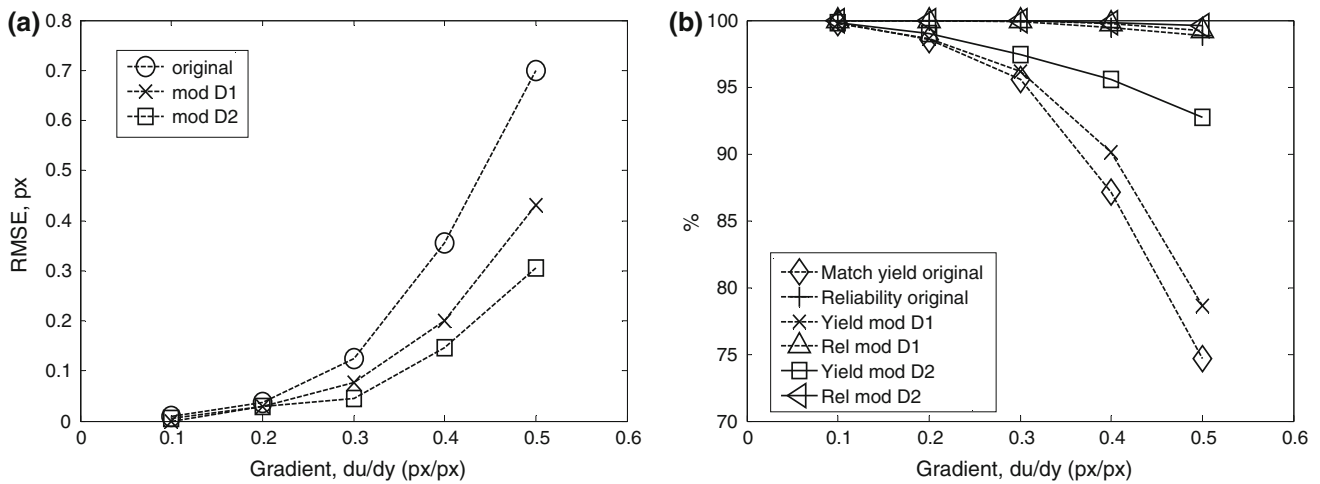

Fig. 6 a RMS error versus flow gradient with a maximum velocity of 25 pixels ($d^* = 0.23$), and **b** match yield and reliability percentages versus gradient using the original and displacement-shifted matching methods

In Lei et al. (2012), synthetic images generated using a moving wall flow, or Stokes' first problem, were processed. These images were also processed using the displacement-shifted matching, but results are not recorded. The original method already provided RMS errors below 0.1 px, match yields of over 98 % and matches with reliabilities of over 99.6 %, and the modifications provided little or no improvement. The majority of particle locations change either not at all or negligibly between the image frames, and for this reason, it would not be expected that there would be a large difference between the original method, which favors a close match to a distant one, and the displacement-shifted methods. Similarly, standard images from the Visualization Society of Japan (Okamoto et al. 2000) were processed, but because they contain displacements no larger than 10 pixels ($d^* = 0.58$), and gradients

of approximately 0.2 px/px or less, little improvement over the results recorded in Lei et al. (2012) was expected or seen.

In order to fully utilize the directional guidance provided by the second modification, synthetic images are generated using a two-dimensional Oseen vortex flow described as

$$u_\theta = \frac{\Gamma}{2\pi r}\left(1 - e^{-\frac{r^2}{\gamma}}\right). \tag{10}$$

Radial velocity is zero, $\Gamma = 5{,}000\pi$, $\gamma = 5{,}000$, and r is the radial distance from the center of the vortex. Displacements in this flow vary from 0 to 22 pixels ($d^* > 0.26$) and gradients ($\partial u_\theta/\partial r$) vary from near zero to 0.5 px/px. The RMS errors from matching results are presented as bar charts in Fig. 7. Three cases are shown for
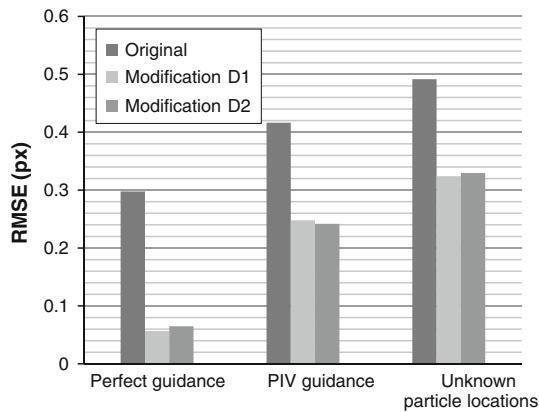
Fig. 7 RMS error of VB-PTV results for a 2D Oseen vortex flow using original and displacement-shifted matching

each matching method: one with known particle locations and the regular PIV guidance used in constructing the proximity matrix, G_{ij}; one with known locations and perfect guidance using the analytic flow solutions to construct G_{ij}; and one with unknown particle locations and regular PIV guidance. The match yield and reliability percentages were generally unchanged or slightly improved by the displacement-shifted approach.

There does not seem to be a clear difference between the performance from modifications D1 and D2 seen in these results, but both displacement-shifted approaches clearly result in improved performance when compared with the original matching method. The improvements to the matching algorithm reduce the RMS error for an Oseen vortex flow by as much as 80 % in the idealized case of perfect guidance, by more than 40 % when PIV guidance is used with known particle locations, and by 33 % when particle locations must be identified.

5 Results from experimental images

The last validation of the modified methods is to apply the methods to real experimental images. The modified methods were first tested with the same shear layer images used in Lei et al. (2012). All three algorithms were applied to the experimental images, and the particle locations were found using the method described in the previous work (Lei et al. 2012). The parameters used in modification D1 and D2 are the same as used in the synthetic image tests. The resulting velocity fields from different methods are overlaid and shown in Fig. 8a and a zoom-in view in Fig. 8c. The maximum velocity gradient and velocity in the shear layer images were 0.08 px/px and 4.44 px ($d* = 2.17$). The original and modified methods gave almost the same results, with only a few vectors difference. Similar to the

synthetic image tests, the performances of the matching methods are verified by particle yield and reliability. Because for the experimental images there are no "correct matches" available, the definitions are slightly different to the ones described in the previous sections. The particle yield is defined as number of matches found over the number of particles identified, and the matching reliability is defined as the number of matches found over the number of matches validated by a universal outlier detection method (Duncan et al. 2010). The numbers are listed in Table 1. These results are in agreement with the synthetic image results shown in Fig. 5a, that the performance difference is very small if both the velocity and velocity gradients are small.

An experimental setup to observe the wake region of flow behind a cylinder was then conducted to test the algorithms' performances under higher velocity gradients. A cylinder of 0.25 in. (6.35 mm) diameter was put inside a 6 by 12 in. (15.24 by 30.48 cm) water tunnel with a free-stream flow velocity of 29.7 mm/s. The imaging area was 19.4 by 19.4 mm, chosen right behind the cylinder to capture the flow at the wake region, where the velocity gradient is expected to be the largest. The corresponding Reynolds number is 187. The time interval between the two frames was set to 30 ms to achieve the high maximum displacement condition. The maximum velocity (displacement) and velocity gradient are 59.98 px ($d* = 0.21$) and 0.24 px/px. The resulting velocity fields from different methods are overlaid and shown in Fig. 8b and zoom-in view in Fig. 8d. The particle yield and reliability numbers are listed in Table 1. It can be observed that in the center of the wake region, the flow is highly rotational. In the region near free stream, the flow has a strong shear. With large displacement and high gradient, these regions can be difficult for the matching algorithms to work. However, a zoom-in look at the wake region (indicated by the red rectangle in Fig. 8b and the results are listed in Table 1) shows that the performance is at the same level as the results from the full image.

The performance numbers in Table 1 of the two different experimental image sets are in agreement with the synthetic image test results shown in Sect. 4. The performance differences between the modified methods and the original method are small for the shear layer images, because the velocity gradient and maximum velocity (displacement) are both small, which corresponds to the similar trends of the 7 px test results shown in Fig. 5b. Modifications D1 and D2 provide a better yield than the original method when both the maximum velocity and gradient are large, correspond to the similar trends of the 25 px test results shown in Fig. 6b. Modification D2 has a greater improvement (+4.57 %) compared with modification D1 (+3.05 %) in yield, and slightly higher in
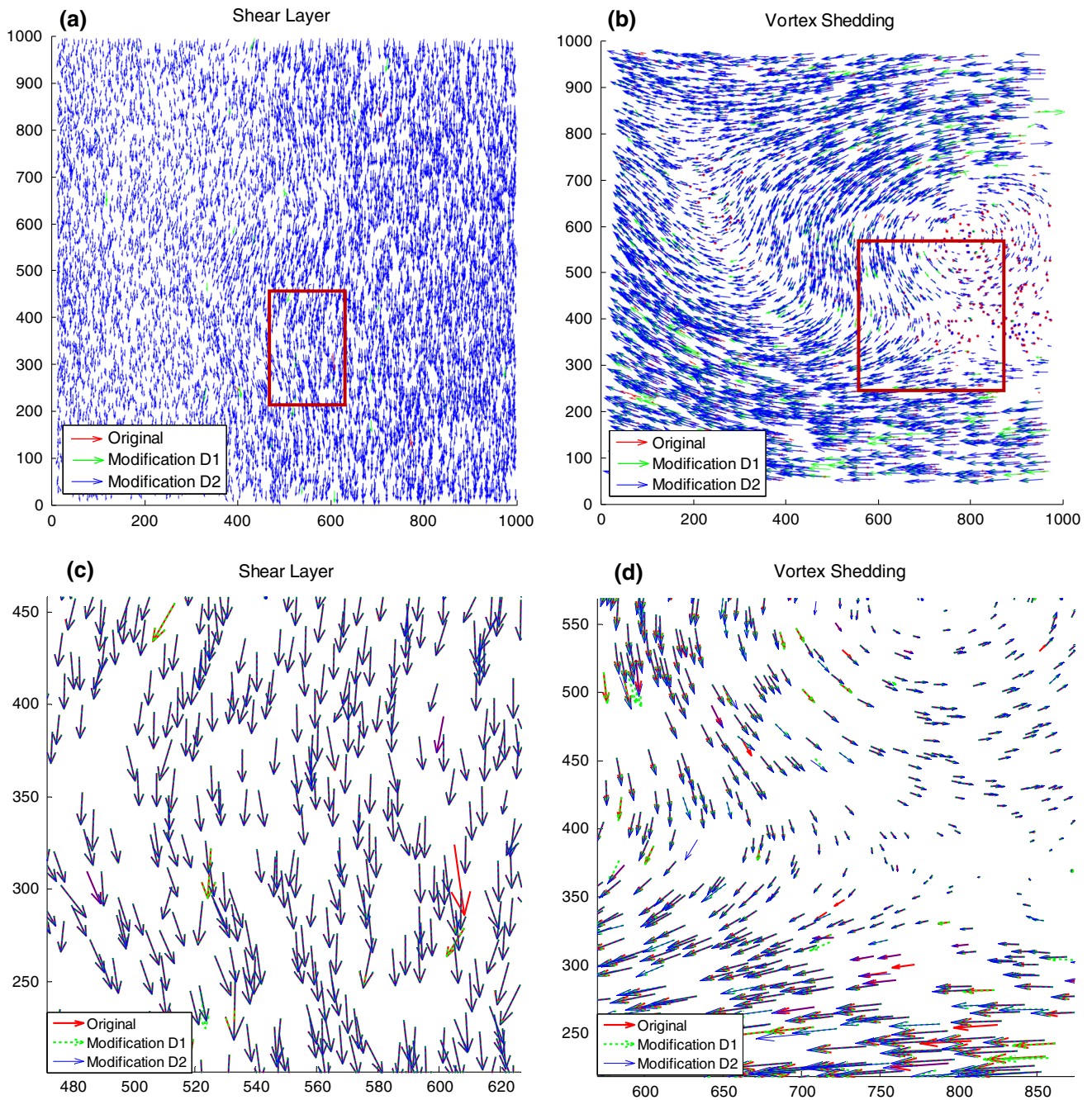
Fig. 8 Vector fields found by different matching methods of experimental images: **a** shear layer, **b** vortex shedding behind a cylinder, **c** zoom-in view of shear layer, **d** zoom-in view of vortex shedding behind a cylinder. The *red rectangular* indicates the "wake region" calculated in Table 1

Table 1 Comparison of the performances results of experimental images

	Particle yield			Reliability		
	Original (%)	Modification D1 (%)	Modification D2 (%)	Original (%)	Modification D1 (%)	Modification D2 (%)
Shear layer	67.36	67.41	67.44	98.94	98.94	98.94
Vortex shedding	57.39	60.44	61.96	99.62	99.56	99.77
Vortex shedding (wake)	62.76	65.41	67.14	99.65	99.66	99.81

reliability. Both improvements are due to the addition of the directional measure to increase the matching robustness.

6 Conclusions and recommendations

The vision-based PTV technique developed in Lei et al. (2012) relied on the principle of proximity, which favored short matches over long ones, and also on the principles of exclusion and similarity. Instead of relying on the principle of proximity to the particle location, the displacement-shifted addition in this paper applies the proximity principle to the displaced particle location based on PIV results, utilizing the guidance of PIV more efficiently. The benefit of using these displacement-shifted approaches in comparison with the original approach is that results are noticeably improved for high gradient flows (0.3 px/px and higher) without affecting results for lower gradient flows. In the synthetic image tests, both displacement-shifted approaches show noticeably reduced RMS errors, and the second approach shows a noticeable improvement in its yield data at the higher gradients. The methods are verified with experimental image sets, and the results are in agreement with the synthetic tests. These improvements are simple to implement, expand the range of flows for which VB-PTV is useful, and recommended in future applications of VB-PTV.

References

Adrian RJ, Westerweel J (2011) Particle image velocimetry. Cambridge University Press, Cambridge

Barnard ST, Thompson WB (1980) Disparity analysis of images. Pattern Anal Mach Intell IEEE Trans 4:333–340

Dabiri D (2006) Cross-correlation digital particle image velocimetry—a review. In: Freire AS, Iiha A, Breidenthal B (eds) Turbulencia. ABCM, Curitiba, pp 155–199

Duncan J, Dabiri D, Hove J, Gharib M (2010) Universal outlier detection for particle image velocimetry (PIV) and particle tracking velocimetry (PTV) data. Meas Sci Technol 21(5):057002

Lei Y-C, Tien W-H, Duncan J, Paul M, Ponchaut N, Mouton C, Dabiri D, Rösgen T, Hove J (2012) A vision-based hybrid particle tracking velocimetry (PTV) technique using a modified cascade-correlation peak-finding method. Exp Fluids 53(5): 1251–1268

Ohmi K, Sapkota A (2006) Cellular neural network based PTV. In Proceedings of 13th international symposium on applications of laser techniques to fluid mechanics 16

Okamoto K, Nishio S, Saga T, Kobayashi T (2000) Standard images for particle-image velocimetry. Meas Sci Technol 11(6): 685–691

Pilu M (1997) A direct method for stereo correspondence based on singular value decomposition. In: Computer vision and pattern recognition, 1997. Proceedings, 1997, IEEE Computer Society Conference on. IEEE, pp 261-266

Raffel M, Willert C, Kompenhans J (1998) Particle image velocimetry: a practical guide. Springer, Berlin

Schonemann P (1966) A generalized solution of the orthogonal procrustes problem. Psychometrika 31:1–10

Scott G, Longuet-Higgins H (1991) An algorithm for associating the features of two images. Proc R Soc Lond B Biol Sci 244(1309): 21–26

Ullman S (1979) The interpretation of visual motion. MIT Press, Cambridge